Applied Surface Science 388 (2016) 268–273

Contents lists available at ScienceDirect

Applied Surface Science

journal homepage: www.elsevier.com/locate/apsusc

Design of a superhydrophobic and superoleophilic film using cured fluoropolymer@silica hybrid

Hao Yang[a], Pihui Pi[b], Zhuo-ru Yang[b], Zhong Lu[a], Rong Chen[a,*]

[a] Key Laboratory for Green Chemical Process of Ministry of Education and School of Chemistry and Environmental Engineering, Wuhan Institute of Technology, Xiongchu Street, Wuhan, 430073, PR China
[b] School of Chemistry and Chemical Engineering, South China University of Technology, Guangzhou, 510640, PR China

ARTICLE INFO

Article history:
Received 13 October 2015
Received in revised form 12 January 2016
Accepted 12 January 2016
Available online 14 January 2016

Keywords:
Superhydrophobic
Superoleophilic
Fluoropolymer
Silica
Hybrid
Oil/water separation

ABSTRACT

Recently, considerable efforts have been made on superhydrophobic–superoleophilic filter to satisfy the requirements of the applications to oil/water separation. In this work, we obtained a superhydrophobic and superoleophilic film by coating cured fluoropolymer@silica hybrid on stainless steel mesh. Fourier transform infrared spectroscopy (FT-IR), X-ray photoelectron spectroscopy (XPS) and thermogravimetric-differential scanning calorimetry (TG-DSC) were used to determine the chemical composition and thermal stability of the sample. The effect of silica nanoparticles (NPs) concentration on the surface property of the hybrid film was analyzed by scanning electron microscopy (SEM), atomic force microscopy (AFM) and contact angle analyzer. The results indicate that silica NPs not only enhance the thermal stability, but also strengthen the hydrophobicity and oleophilicity of the film. When 20 wt% silica NPs was added into the thermosetting fluoropolymer, the hybrid film shows both superhydrophobicity and superoleophilicity owing to the large surface roughness factor (RMS) and porous structure. Moreover, the hybrid film could be used to separate water from different oils effectively. When the pore size of the mesh is less than 300 μm, the oil/water separation efficiency of the film reaches above 99%, which shows a great potential application to dehydrate fuel oils.

1. Introduction

With the development of aviation and automobile industry, the requirement of engine in planes or cars is higher and higher. Oil, as "blood" in engine, plays a crucial and important role in operational life span and service efficiency of engine. However, oil in engine usually contains some water, which can accelerate the deterioration of oil and destroy the engine. Therefore, the effective removal of water from oil is a big issue for modern industry. Among oil/water separation technologies, coalescence separation technology has been widely used in virtue of its large processing capacity and low energy consumption and economic cost [1]. As the illustration of the operation principle of a coalescence separator in Scheme 1, the mixture of oil and water first passes through a coalescer filter to form large water droplets to break the emulsion. Then the separation of water and oil was achieved under gravity by a separating filter. Usually, the separation filter is made by hydrophobic and oleophilic materials coated on metal meshes, and the oil/water separation efficiency is highly related to its wettability [2]. Recently, many works have been devoted to the preparation of superhydrophobic-superoleophilic films for their exciting applications in oil/water separation [3,4]. Among the reported films, inorganic nanomaterials such as SiO_2 [5–7], TiO_2 [8,9], ZnO nanorod [10–12], carbon nanotube [13,14], copper hydroxide nanowire [15,16], etc. are commonly used, because they could construct micro-nano binary structures for the sake of superhydrophobicity or superoleophilicity. However, some prepared superhydrophobic films are not stable, especially in high hydraulic pressure of the flow of oil/water mixture. In addition, some nanoparticles are prone to be detached from the substrate, which may cause wear and tear on the engine. Therefore, developing a stable superhydrophobic and superoleophilic film that makes nanoparticles firmly attach on the substrate is emergent and necessary for practical application [7,17,18]. In our previous work, we fabricated silica film with superhydrophobicity and superoleophilicity on stainless steel mesh, which proved the oil/water separation capacity [19,20]. However, the adhesion force between silica nanoparticles (NPs) and mesh was weak because of the lack of chemical band between them. Further, we incorporated fluorinated polymers with silica NPs to fabricate composite films to solve this problem, and found that the

* Corresponding author. Tel.: +86 13659815698; fax: +86 2787195671.
E-mail address: rchenhku@hotmail.com (R. Chen).

http://dx.doi.org/10.1016/j.apsusc.2016.01.099
0169-4332/

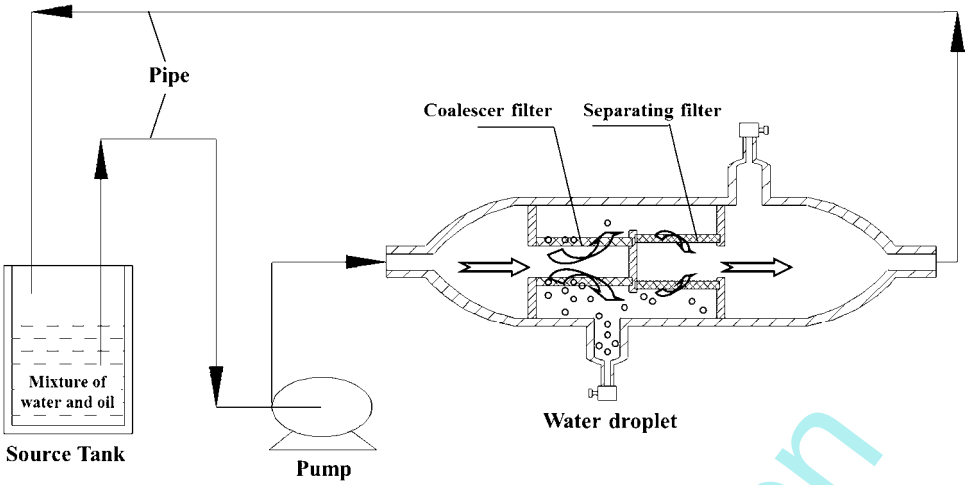

Scheme 1. Schematic diagram of a coalescence separator for oil/water separation.

chemical composite of the fluorinated polymers could switch the wettability of the film [21]. In this paper, we investigated the effect of silica NPs on the wettability of the composite films in detail, and determined the oil/water separation efficiency of the films under different conditions.

2. Experimental

2.1. Materials

Methyl methacrylate (MMA), stearyl methacrylate (SMA) and 2-hydroxyethyl methacrylate (HEMA) were purchased from Guangzhou Shuangjian Trading Co., Ltd., China. Perfluoroalkyl ethyl methacrylates ($C_nF_{2n+1}CH_2CH_2OOC(CH_3)C{=}CH_2$ (n = 6,8,10), FMA) was from Shanghai Fchemicals Technology Co., Ltd., China. Silica aerogel (R974, hydrophobically modified by dimethyldichlorosilane DDS) was from Degussa Evonik. HDI trimer was purchased from Bayer. 2,2-azobisisobutyronitrile (AIBN) was from Tianjin Kemiou Chemical Reagent Co., Ltd and recrystallized before use. Stainless steel mesh, petrol, kerosene, diesel and hydraulic oil were purchased from local market.

2.2. Preparation of fluoropolymer@silica hybrid film

In a typical experiment, 5 g FMA was added into 50 g solution of butyl acetate and xylene (V/V=1:1) with vigorous stirring and refluxed at 80 °C for 30 min. Then 20 g MMA, 15 g SMA, 10 g HEMA and 0.75 g AIBN were mixed, followed by adding the mixture slowly into the reaction system dropwise within 2 h. After 4 h refluxing of the reaction mixture at 80 °C, fluoropolymer was obtained.

The fluoropolymer@silica hybrid films were prepared by mixing 10 g fluoropolymer and different weights of silica aerogel in 190 g solution of butyl acetate and xylene (V/V = 1:1), then 1 g HDI trimer was added with continuous stirring, finally the stainless steel mesh were put into the mixtures and cured at 110 °C for 2 h.

2.3. Characterization

The chemical compositions of silica, fluoropolymer and fluoropolymer@silica hybrid were characterized by Fourier transform infrared spectroscopy (FTIR, Vector 33, Bruker, Germany). X-ray photoelectron spectroscopy (XPS) data were collected in both survey and high-resolution mode on Kratos Axis Ultra DLD systems equipped with Al K α X-ray source and operating at 300 W. The surface morphology of hybrid film was observed by scanning electron microscopy (SEM, LEO 1530VP, Germany). The surface roughness of the hybrid was characterized by atomic force microscope (AFM, CSPM5000, Benyuan, China). The thermal stability of fluoropolymer and fluoropolymer@silica hybrid were computed by thermogravimetric-differential scanning calorimetry (TG-DSC, Netzsch STA449C, Germany) by heating the sample (8 mg) in a flow of air (30 mL/min) at 10 °C/min from room temperature to 600 °C. Static contact angle (CA) measurements were performed with an optical contact angle meter (OCA20 Micro, Dataphysics, Germany). The wettability of the hybrid films was determined by measuring CAs of two probe liquids: water and kerosene.

3. Results and discussion

Fig. 1 shows FTIR spectra of silica, fluoropolymer and fluoropolymer@silica hybrid. In the IR spectrum of silica, two characteristic peaks at 3436 and 1631 cm^{-1} were ascribed to physically absorbed water. Three peaks at 1108, 811 and 474 cm^{-1} were attribute to absorption peak of Si-O-Si band. No peak at 960 cm^{-1} was observed, indicating the absence of Si-OH group. Besides, the weak peak emerging at 2967 cm^{-1} could be ascribed to stretching vibration of C-H band, indicating that the hydrophobic silica NPs were modified by alkyl groups. In the IR spectrum of fluoropolymer, three peaks at 2992, 2926 and 2854 cm^{-1} were associated with methyl or methylene groups. The strong peak at 1731 cm^{-1} was ascribed to the stretching vibration of carbonyl group, indicating the presence of methacrylate. Two peaks at 1452 and 1388 cm^{-1} were characteristic peaks of MMA, and another two peaks at 1243 and 1151 cm^{-1} were attributed to —CF_2 and —CF groups from FMA. The peak at 750 cm^{-1} could be ascribed to —$(CH_2)_n$— ($n \geq 4$) groups from SMA. At 3524 cm^{-1}, the absorption band belonged to stretching vibration of -OH group from HEMA. Meanwhile, the double bond at 1640 cm^{-1} did not appear, which implied that MMA, SMA, FMA and HEMA monomers have been copolymerized. The above data demonstrated that the fluoropolymer consisted of MMA/SMA/HEMA/FMA. Compared with silica and fluoropolymer spectra, some new peaks emerged in fluoropolymer@silica spectrum. For example, the peak at 3397 cm^{-1} was ascribed to —NH group, and the peak at 1735 cm^{-1} was ascribed to —NH—COO— group. Another two peaks at 1692 and 1529 cm^{-1} belonged to —NH—CO—NH— group and —C—N— group, respectively, which demonstrated the characteristic groups of polyurethane. The weak peak at 2277 cm^{-1} was ascribed to the remaining —NCO— group from HDI trimer. Besides, the peak at 3524 cm^{-1} in fluoropolymer disappear in fluoropolymer@silica hybrid, which proves

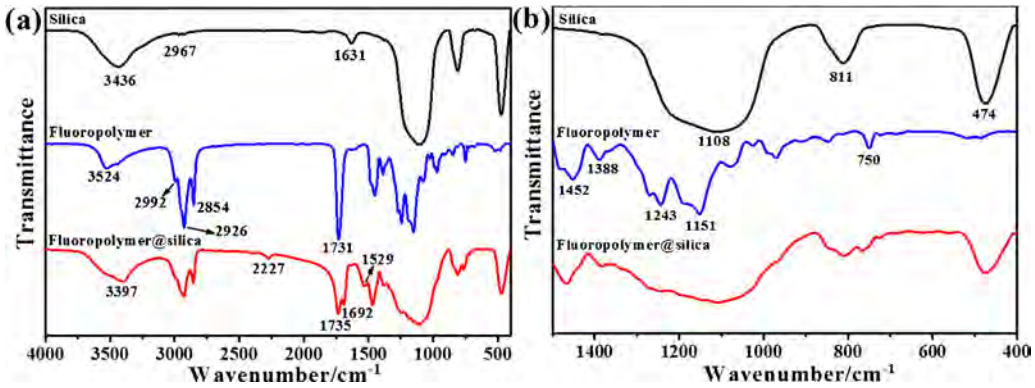

Fig. 1. FTIR spectra of silica, fluoropolymer and fluoropolymer@silica hybrid. b is partial magnified image of a.

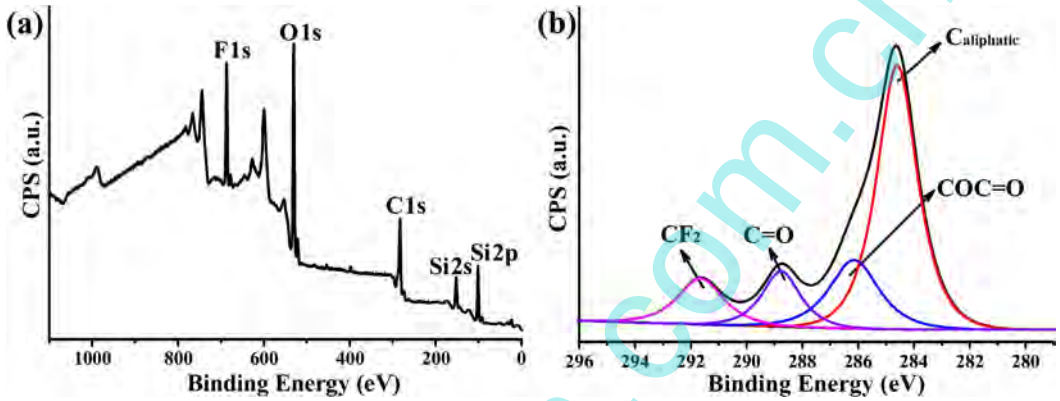

Fig. 2. XPS spectra of fluoropolymer@silica hybrid film (a: survey; b: C 1s).

that the hydroxyl group in fluoropolymer has reacted with isocyanate of the curing agent. Because of the lacking of Si—OH group on the silica surface, the silica NPs were physically integrated into the coating during the curing process.

The surface chemical composite of the fluoropolymer@silica hybrid film was further measured by XPS analysis. As shown in Fig. 2, there were four kinds of elements on the surface of the film. The atom concentration of C, O, F, and Si elements were 37.6%, 25.7%, 10.3% and 26.4%, respectively. C was the major element, which was from both fluoropolymer and surface alkyl group of silica NPs. The strong peak located at 284.6 eV of C 1s spectrum could be ascribed to $C_{aliphatic}$ group from SMA (Fig. 2b), which resulted in hydrophobic and oleophilic properties of the film. Although the concentration of F element (from FMA) was the minimum, it could dramatically decrease the surface free energy of the film and enhance the film hydrophobicity.

The fluoropolymer film coated on stainless steel mesh exhibited water contact angle (CA) 125.7° and kerosene CA 27.9°, respectively (Fig. 3), which showed hydrophobicity and oleophilicity. According to Wenzel theory, roughness can strengthen the wetting properties, so it can be speculated that increasing the roughness of the surface, superhydrophobic and superoleophilic surface can be obtained on a pristine hydrophobic and oleophilic surface. Based on the previous works, constructing enough rough surface is significant to fabricate superhydrophobic surface [22,23], and silica NPs are usually used to create such surfaces [24,25]. Therefore, we tried to adjust the dosage of the silica NPs to obtain appropriate roughness of the surface for superhydrophobic and superoleophilic film.

Fig. 3 shows water and oil CAs of fluoropolymer@silica hybrid films on stainless steel mesh with different silica NPs addition. With the silica NPs dosage increased, the water CA increased while oil CA decreased, which fit to Wenzel theory. When the silica NPs dosage was 20%, the water CA raised to 150.5° and oil CA decreased to 4.2°, which proved to be superhydrophobicity and superoleophilicity. Further increasing the silica NPs to 25%, the water CA reached the highest value at 157.4°, and oil droplet could spread quickly on the surface, with nearly 0° of oil CA.

The surface morphology and roughness of the hybrid films with different silica NPs dosage were characterized by SEM and AFM images. Fig. 4 showed the surface morphology of the hybrid films consisted of different silica concentrations range from 0 to 25 wt%. The fluoropolymer film without silica NPs displayed smooth surface (Fig. 4a). With the increase of silica concentration, more and more silica NPs covered the stainless steel wire, and the packing density of the silica also increased. When the silica concentration was 10%, uniform silica NPs were well-dispersed on the wire with some

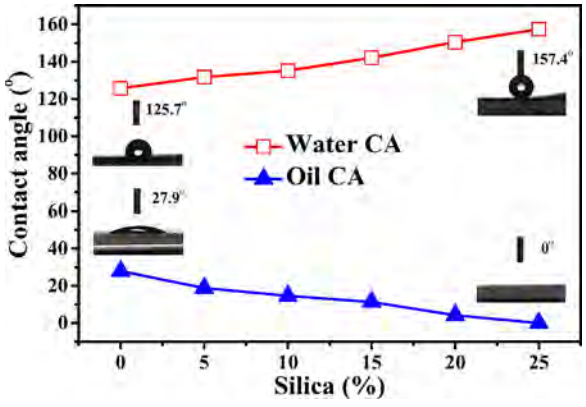

Fig. 3. Water and kerosene CAs of fluoropolymer@silica hybrid films on stainless steel mesh with different silica dosage (The pore size of the mesh is 75 μm).

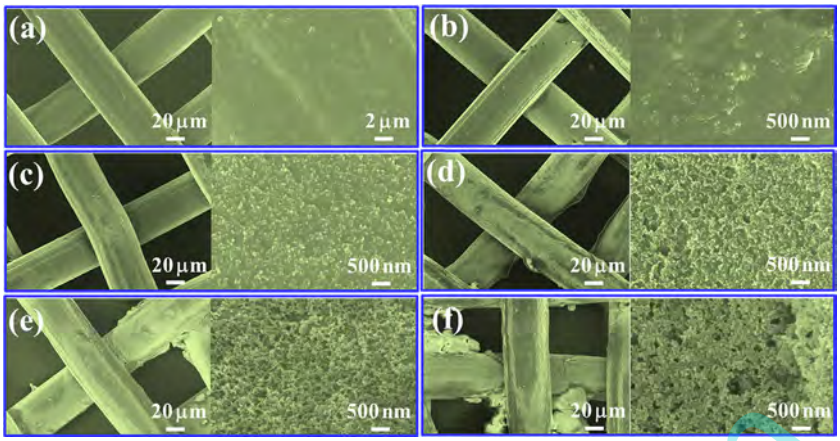

Fig. 4. SEM images of fluoropolymer@silica hybrid film on stainless steel mesh with 0% (a), 5% (b), 10% (c), 15% (d), 20% (e) and 25% (f) silica addition.

gaps. Further increasing the concentration to 15%, dense silica film was formed on the wire and some porous structures appeared on the packed nanoparticles. Further increasing the concentration to 20%, the thickness of the film increased and more porous structures dispersed on the surface. When the silica concentration reached 25%, the silica NPs aggregated seriously, which blocked the pore structure of the mesh (Fig. 4f).

The surface roughness of the hybrid films with different silica NPs dosage was analyzed by AFM, as depicted in Fig. 5. The root mean square (RMS) values of the films increased with the increase of silica concentration. When the substrate was covered only by fluoropolymer, the surface was very smooth, and almost no any fluctuation was observed (Fig. 5a). When the silica concentration was 5%, some tiny peaks represented of silica NPs emerged randomly on the surface (Fig. 5b). Further increasing the silica concentration to 10%, many tiny peaks dispersed on the surface, and there also existed a few mountain, which was composed of many

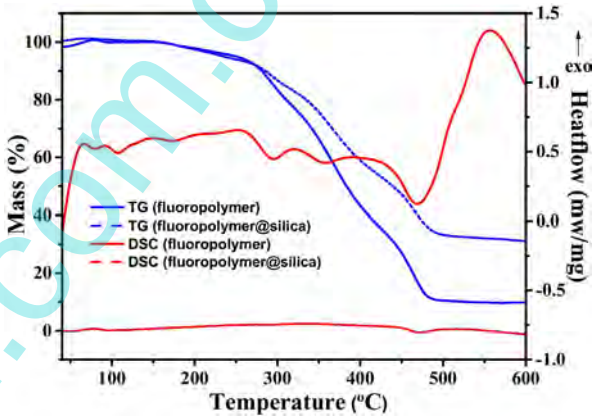

Fig. 6. TG-DSC curves of fluoropolymer and fluoropolymer@silica hybrid.

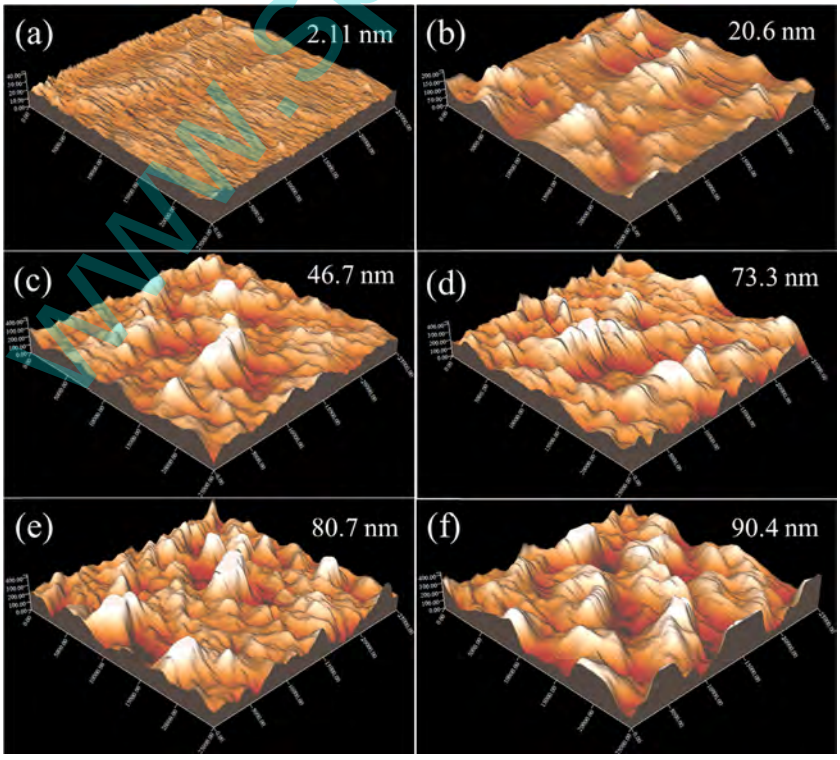

Fig. 5. 3D AFM images of fluoropolymer@silica hybrid films with 0% (a), 5% (b), 10% (c), 15% (d), 20% (e) and 25% (f) silica addition. The insets are the RMS values of the films.

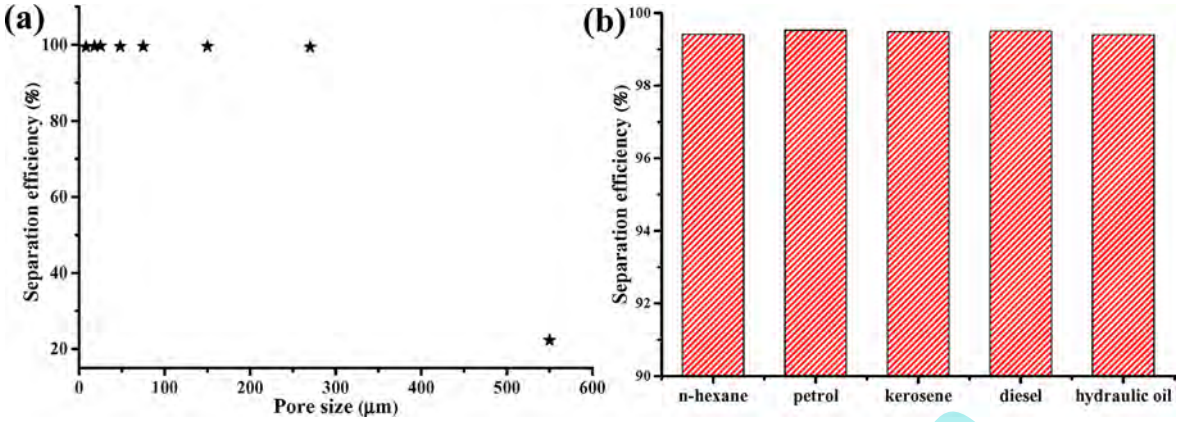

Fig. 7. The separation efficiency of the superhydrophobic-superoleophilic films for water and kerosene with different pore size of meshes (a) and separation efficiency of mixtures of the water and different oils with 75 μm pore size of mesh (b).

silica aggregates (Fig. 5c). Continuing increasing silica addition, the amount of mountain increased and they were dispersed uniformly. AFM results indicated that the film showed both micro-scale aggregates and nano-scale silica NPs if adding enough silica NPs, similar with the lotus leave.

From the analysis above, it was proposed that the formation of superhydrophobic and superoleophilic fluoropolymer@silica hybrid film could be ascribed to two factors. Firstly, the desired chemical composition benefited the flat film hydrophobic and oleophilic. Secondly, the bionic nanostructure improved both the hydrophobicity and oleophilicity. Such a film could repel water droplets easily, and the porous structure of the silica aggregate made oil absorbable in the holes by capillary force. It is noticeable that when the silica concentration was 25%, the surface showed maximum water CA and minimum oil CA. However, the decreased pore size of the mesh would increase the resistant force of oil penetrating the mesh, so we chose the hybrid film with 20% silica concentration for further oil/water separation application.

The as-prepared fluoropolymer@silica hybrid film also showed enhanced thermal stability than that of fluoropolymer. As shown in Fig. 6, the fluoropolymer exhibited a slight endothermic peak at 292.1 °C in DSC curve, when the weight loss of the polymer was 13.39%. It might be attributed to the decomposition of low molecule. The strong endothermic peak appeared at 470.3 °C when the organic polymer was degraded dramatically, and the weight of residues of the polymer was only 9.75% at 600 °C. Compared with the fluoropolymer, there was no obvious endothermic peak in DSC curve of the hybrid, and its weight loss decreased more slowly because of the cross-linked chemical band and the addition of silica NPs. The weight of residues of the hybrid was 31.14% at 600 °C. It was 21.39% higher than that of fluoropolymer, which was almost the same with the 20% silica addition.

To evaluate the oil/water separation property of the superhydrophobic and superoleophilic fluoropolymer@silica hybrid films, we measured the corresponding oil/water separation efficiencies with different pore sizes of the meshes, which is displayed in Fig. 7a. When the pore size was larger than 300 μm, the hydrophobic force that was provided by the hybrid film was not large enough to support the water drop, and made water pass through the mesh. When the pore size was less than 300 μm, the separation efficiencies of all the films were above 99%, and the pore size had little influence on the separation capability. Furthermore, different oils such as n-hexane, petrol, kerosene, diesel and hydraulic oil were taken to measure the separation efficiency of the film with 75 μm pore size. Although different oils have different surface tension and viscosity, the superhydrophobic-superoleophilic films showed excellent oil/water separation efficiencies for all the tested liquids (Fig. 7b).

4. Conclusion

In summary, cured fluoropolymer@silica films with both superhydrophobicity and superoleophilicity were successfully prepared on the stainless steel mesh. The results showed that FMA and SMA monomers made flat fluoropolymer hydrophobic and oleophilic, and the addition of silica NPs increased the surface roughness of the film and enhanced its wettability. When the silica concentration was 20%, the film showed water CA of 150.5° and oil CA of 4.2°, as well as good thermal stability. The hybrid film exhibited excellent oil/water separation performances. The oil/water separation efficiencies were higher than 99% with different mixtures of water and oils when the pore size of mesh was less than 300 μm.

Acknowledgements

This work was supported by the National Natural Science Foundation of China (Grant 21201135, 21471121), High-Tech Industry Technology Innovation Team Training Program of Wuhan Science and Technology Bureau (2014070504020243), Program for Excellent Talents of Hubei Provincial Department of Education (Q20121502) and Scientific Research Foundation of Wuhan Institute of Technology.

References

[1] T. Frising, C. Noik, C. Dalmazzone, The liquid/liquid sedimentation process: From droplet coalescence to technologically enhanced water/oil emulsion gravity separators: A review, J. Disper. Sci. Technol. 27 (2006) 1035–1057.
[2] S. Agarwal, V. von Arnim, T. Stegmaier, H. Planck, A. Agarwal, Role of surface wettability and roughness in emulsion separation, Sep. Purif. Technol. 107 (2013) 19–25.
[3] Z.X. Xue, Y.Z. Cao, N. Liu, L. Feng, L. Jiang, Special wettable materials for oil/water separation, J. Mater. Chem. A 2 (2014) 2445–2460.
[4] B. Wang, W.X. Liang, Z.G. Guo, W.M. Liu, Biomimetic super-lyophobic and super-lyophilic materials applied for oil/water separation: a new strategy beyond nature, Chem. Soc. Rev. 44 (2015) 336–361.
[5] C.H. Xue, P.T. Ji, P. Zhang, Y.R. Li, S.T. Jia, Fabrication of superhydrophobic and superoleophilic textiles for oil-water separation, Appl. Surf. Sci. 284 (2013) 464–471.
[6] F. Liu, M.L. Ma, D.L. Zang, Z.X. Gao, C.Y. Wang, Fabrication of superhydrophobic/superoleophilic cotton for application in the field of water/oil separation, Carbohyd. Polym. 103 (2014) 480–487.
[7] X. Zhang, T. Geng, Y.G. Guo, Z.J. Zhang, P.Y. Zhang, Facile fabrication of stable superhydrophobic SiO_2/polystyrene coating and separation of liquids with different surface tension, Chem. Eng. J. 231 (2013) 414–419.
[8] C.R. Gao, Z.X. Sun, K. Li, Y.N. Chen, Y.Z. Cao, S.Y. Zhang, L. Feng, Integrated oil separation and water purification by a double-layer TiO_2-based mesh, Energy Environ. Sci. 6 (2013) 1147–1151.
[9] J.Y. Huang, S.H. Li, M.Z. Ge, L.N. Wang, T.L. Xing, G.Q. Chen, X.F. Liu, S.S. Al-Deyab, K.Q. Zhang, T. Chen, Y.K. Lai, Robust superhydrophobic TiO_2@fabrics

for UV shielding, self-cleaning and oil-water separation, J. Mater. Chem. A 3 (2015) 2825–2832.
[10] D.L. Tian, X.F. Zhang, J. Zhai, L. Jiang, Photocontrollable water permeation on the micro/nanoscale hierarchical structured ZnO mesh films, Langmuir 27 (2011) 4265–4270.
[11] H. Li, Y.S. Li, Q.Z. Liu, ZnO nanorod array-coated mesh film for the separation of water and oil, Nanoscale Res. Lett. 8 (2013) 1–6.
[12] D.L. Tian, X.F. Zhang, X. Wang, J. Zhai, L. Jiang, Micro/nanoscale hierarchical structured ZnO mesh film for separation of water and oil, Phys. Chem. Chem. Phys. 13 (2011) 14606–14610.
[13] C.H. Lee, N. Johnson, J. Drelich, Y.K. Yap, The performance of superhydrophobic and superoleophilic carbon nanotube meshes in water-oil filtration, Carbon 49 (2011) 669–676.
[14] J.C. Gu, P. Xiao, J. Chen, J.W. Zhang, Y.J. Huang, T. Chen, Janus polymer/carbon nanotube hybrid membranes for oil/water separation, ACS Appl. Mater. Interfaces 6 (2014) 16204–16209.
[15] F. Zhang, W.B. Zhang, Z. Shi, D. Wang, J. Jin, L. Jiang, Nanowire-haired inorganic membranes with superhydrophilicity and underwater ultralow adhesive superoleophobicity for high-efficiency oil/water separation, Adv. Mater. 25 (2013) 4192–4198.
[16] D.D. La, A.N. Tuan, S. Lee, J.W. Kim, Y.S. Kim, A stable superhydrophobic and superoleophilic Cu mesh based on copper hydroxide nanoneedle arrays, Appl. Surf. Sci. 257 (2011) 5705–5710.
[17] P. Guo, S.R. Zhai, Z.Y. Xiao, Q.D. An, One-step fabrication of highly stable, superhydrophobic composites from controllable and low-cost PMHS/TEOS sols for efficient oil cleanup, J. Colloid Interface Sci. 446 (2015) 155–162.
[18] Q. Zhu, Q.M. Pan, Mussel-inspired direct immobilization of nanoparticles and application for oil-water separation, ACS Nano 8 (2014) 1402–1409.
[19] H. Yang, P.H. Pi, Z.Q. Cai, X.F. Wen, X.B. Wang, J. Cheng, Z.R. Yang, Facile preparation of super-hydrophobic and super-oleophilic silica film on stainless steel mesh via sol-gel process, Appl. Surf. Sci. 256 (2010) 4095–4102.
[20] H. Yang, X.J. Zhang, Z.Q. Cai, P.H. Pi, D.F. Zheng, X.F. Wen, J. Cheng, Z.R. Yang, Functional silica film on stainless steel mesh with tunable wettability, Surf. Coat. Technol. 205 (2011) 5387–5393.
[21] H. Yang, X.J. Hu, R. Chen, S.T. Liu, P.H. Pi, Z.R. Yang, Fluoropolymer/SiO_2 composite films with switchable superoleophilicity and high oleophobicity for “on-off” oil permeation, Appl. Surf. Sci. 280 (2013) 113–116.
[22] C. Yang, U. Tartaglino, B.N.J. Persson, Influence of surface roughness on superhydrophobicity, Phys. Rev. Lett. 97 (2006).
[23] M. Nosonovsky, Multiscale roughness and stability of superhydrophobic biomimetic interfaces, Langmuir 23 (2007) 3157–3161.
[24] W. Ming, D. Wu, R. van Benthem, G. de With, Superhydrophobic films from raspberry-like particles, Nano Lett. 5 (2005) 2298–2301.
[25] S.H. Wang, M. Li, Q.H. Lu, Filter paper with selective absorption and separation of liquids that differ in surface tension, ACS Appl. Mater. Interfaces 2 (2010) 677–683.